The International Journal of Advanced Manufacturing Technology
https://doi.org/10.1007/s00170-018-1602-0

ORIGINAL ARTICLE

Torsion analysis of the anisotropic behavior of FDM technology

Cesar Omar Balderrama-Armendariz[1] · Eric MacDonald[2] · David Espalin[3] · David Cortes-Saenz[1] · Ryan Wicker[3] · Aide Maldonado-Macias[4]

Received: 21 September 2017 / Accepted: 10 January 2018

Abstract
Several reports have studied the mechanical properties of the material extrusion additive manufacturing process, specifically referred to as fusion deposition modeling (FDM) developed by Stratasys. As the applications for 3D printed parts continue to grow in diversity (e.g., gears, propellers, and bearings), the loading conditions applied to printed parts have become more complex, and the need for thorough characterization is now paramount for increased adoption of 3D printing. To broaden the understanding of torsional properties, this study focused on the shear strength of specimens to observe the impact from additive manufacturing. A full factorial (4^2) design of experiments was used, considering the *orientation* and the *raster angle* as factors. XYZ, YXZ, ZXY, and XZY levels were considered for the orientation parameter, as well as 0°, 45°, 90°, and 45°/45° for the raster angle parameter. Ultimate shear strength, 0.2% yield strength, shear modulus, and fracture strain were used as response variables to identify the most optimal build parameters. Additionally, stress-strain diagrams are presented to contrast elastic and plastic regions with traditional injection molding. Results demonstrated an interaction of factors in all mechanical measured variables whenever an orientation and a raster angle were applied. Compared to injection molding, FDM specimens were similar for all measured torsion variables except for the fracture strain; this led to the conclusion that the FDM process can fabricate components with similar elastic properties but with less ductility than injection molding. The orientation in YXZ with the raster angle at 0^0 resulted in the most suitable combination identified in the response optimization analysis.

Keywords Torsion test · Additive manufacturing · Anisotropy · Fused deposition modeling · Stress strain · ABS

1 Introduction

Additive manufacturing (AM) has been gaining ground in the last decade through the introduction of new platforms for the fabrication of prototypes and, more recently, of functional components for specialized industries including the biomedical and aerospace ones. Due to the reduced cost of thermoplastic materials (particularly when compared to metals or photocurable resins) and to the introduction of affordable desktop printers, thermoplastic material extrusion printing is being used in many factories, schools and even homes. For example, worldwide sales estimates for 2016 were of 455,772 units, more than twice the 219,168 units shipped in 2015 [1]. Of the seven process categories developed by the ASTM F2792-12a [2], material extrusion AM has been forecasted to lead market sales through 2020 [1].

Despite the fact that FDM has a lot of applications, standardization for the mechanical properties of printed parts is difficult to establish. Even the same object can have different mechanical behavior when printed in different orientations. Thus, determining printer parameters according to the target functionality is required to ensure the correct operation of the objects and endure the external and internal mechanical forces. One of the forces involved in many practical applications, and little explored for 3D printed thermoplastics, is torsion [3]. Many products involving rotation require specifications for torque to design components according to the

✉ Cesar Omar Balderrama-Armendariz
cesar.balderrama@uacj.mx

[1] Rapid Prototyping Laboratory, Universidad Autónoma de Ciudad Juárez, 32310 Ciudad Juárez, Chihuahua, Mexico

[2] Advanced Manufacturing Research Center, Youngstown State University, Youngstown, OH 44455, USA

[3] W. M. Keck Center for 3D Innovation, The University of Texas at El Paso, El Paso, TX 79968, USA

[4] Department of Industrial and Manufacturing Engineering, Autonomous University of Ciudad Juarez, Ave. del Charro 450 Norte, 32310 Ciudad Juarez, Chihuahua, Mexico

Published online: 21 January 2018

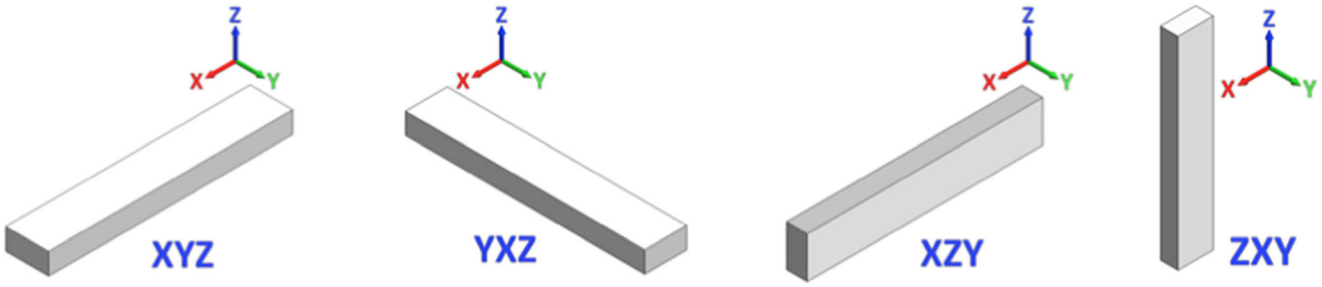

Fig. 1 Orientation of specimens according to the origin in the FDM printer machine

physical properties delivered by the material and process. Manual (wrenches, pliers, drive ratchets, etc.) and electric tools (drills, routers, circular saws, etc.) and fastening elements are examples, as well as components involved used in motors or turbines. In general, any printed part subjected to angular forces will need torsional specifications.

Literature exists which has explored the anisotropic behavior of 3D printed parts through the characterization of materials and physical properties of specimens. Tensile strength and elastic modulus have been reported [4–8] along with compressive strength [9–11], flexure force [11, 12], and impact resistance [13, 14]. Many printing parameters have also been tested to generate more resistant and precise components in FDM technology. Parameters, such as air gap, layer height, offset contours, bed width, build direction, and raster angle, are identified as significant in the optimization of mechanical properties [4, 7–10, 12, 15].

Air gap is one of these significant parameters and represents the space formed between printed rasters on the same layer of a model. In some software, air gap is controlled by the infill parameters. Air gap removal can improve mechanical properties of FDM fabricated parts [7]. A negative air gap leads to more dense components, with higher strength [10] affecting the elastic performance of the compliant ABS prototype [12]. In the case of *layer thickness* (also referred to as layer height), surface roughness is improved [15] through decreases in layer thickness, while elastic performance [12] and strength [3] are improved through increases in layer thickness. The *contour* of a printed piece is the wall generated at the exterior boundary of the structure, which also confines the interior rasters. This exterior boundary can include a single extrusion pass or multiple passes—with additional passes increasing the thickness of the contour. The greater the number of contour passes, the greater the stiffness (as well as the elastic modulus) and the greater the maximum strength [4]. When the number of contour passes increases, the percentage of elongation to failure decreases [10]. *Bead width* is the width of the filament deposited by the nozzle [4]. As the bead width decreases, build time increases; consequently, the production rate is reduced. However, decreases in bead width beneficially improve the surface quality and cause a slight effect on the tensile test [10].

According to literature, air gap, layer height, offset contours, and bead width are measurable parameters that have intuitive behavior, and existing documentation describes optimization for specific applications [8]. Some authors denote that since in FDM every layer is filled by roads according to a certain "path," roads can be considered as the real building units of the process [5]. However, orientation and raster angle are positional parameters that require operator intervention according to the direction of applied forces in the final field application.

Build direction is related to the orientation of the part in the printing chamber of the AM system. Layers are sequentially added in the positive Z (axial) direction. Build direction has been analyzed in terms of compression, highlighting the

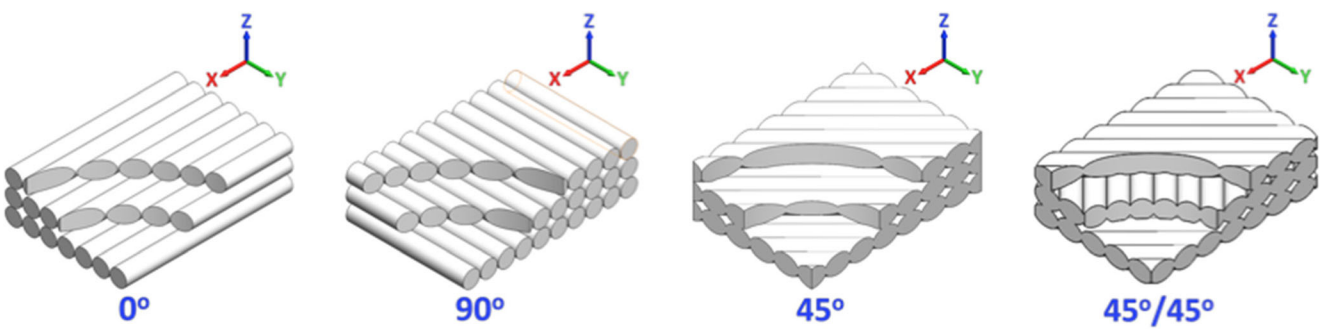

Fig. 2 Representation of direction of rasters (0°, 90°, 45°, and 45°/45°) of the fusion deposition modeling

Table 1 Parameters used to build specimens: (a) Printed specimens parameters on Fortus 400mc; (b) Injection molding parameters on Morgan-Press G-100T

Parameter	Value	Parameter	Value
Part fill style	One raster	Clamp force	11,000 kg
Part interior style	Solid	Pilot valve	6,205.28 Kpa
Contour width	0.00508 mm	Cycle timer	5 s
Raster width	0.00508 mm	Nozzle type	B
Contour to raster air gap	0.0 mm	Barrel temperature	248.89 °C
Raster to raster air gap	0.0 mm	Nozzle temperature	260 °C
Layer thickness	0.00254 mm	Mold temperature	82.22 °C
Number of contours	1		
Number of interior contours	1		
Nozzle temperature	316 °C		
(a)		(b)	

anisotropic behavior of AM fabricated parts in axial and transverse orientation [9]. In terms of impact resistance, a sensitivity also exists toward the build orientation [13], and the strength (tensile) is magnified when the direction of the beads is parallel to that of the load [10]. For practical use, ASTM F2921-11 [16] identified a general orthogonal notation to provide a common framework for describing orientation.

Raster angle is the direction in which the beads or roads are printed according to the position of the part. 0°, 45°, 90°, and 45°/45° are common raster angles used within infill areas. The findings of Ziemian et al. in 2012 [6] refer to the raster angle as having a significant effect on the tensile strength of the FDM specimens. In compression, the 45° raster specimens were significantly weaker, and the three-point bend and impact tests correlate well with tension test results, indicating that the yield strength is the largest for the 0° raster angle. Also, Riley [17] demonstrated that flexural strength was found to be greater than tensile strength for all raster angles considered.

Information on torsion analysis of printed parts is lacking. Torres et al. 2015 evaluated the layer thickness and infill density along with a post processing heat treatment implementation in polylactic acid (PLA) material, which resulted in two parameters being highlighted in the context of optimizing for strength. In the case of heat treatments, slight improvements were seen in the resulting properties. Results indicated that ductility was mainly affected by infill and heat treatment, while layer thickness had only a slight effect on the fracture strain achieved [3].

According to the information presented above, the importance of the printing position lies in the fact that the printed components could have different mechanical strength according to the decisions made prior to printing an object. Consequently, orientation and raster angle could be parameters useful to provide better mechanical characteristics and can be used by component designers as well as those involved in developing new hardware and software for 3D printers.

This research was triggered by the need both to find optimized parameters to obtain the best printing position, and to fill an information gap concerning torsional behavior. Additionally, a comparison with injection molding specimens was used as a baseline in order to understand the performance of 3D printing relative to traditional manufacturing—specifically when considering torsion.

Table 2 Coefficients for rectangular bars in torsion (table constructed by referring to [20])

a/b	c_1	c_2
1	0.208	0.1406
1.2	0.219	0.1661
1.5	0.231	0.1958
2	0.246	0.229
2.5	0.258	0.249
3	0.267	0.263
4	0.282	0.281
5	0.291	0.291
10	0.312	0.312
∞	0.333	0.333

2 Experimental process

Torsional specimens were fabricated using a Stratasys ABS-M30 thermoplastic filament and a Fortus 400mc printer (Stratasys, Ltd., Eden Prairie, MN, USA). A full factorial (4^2) design of experiments with three replicates was used to print 48 specimens using the orientation and the raster angles as factors. XYZ, YXZ, ZXY, and XZY levels (Fig. 1) were used as most common orientations from ASTM F2921-11 [16], and four raster angle levels were also considered—0°, 45°, 90°, and 45/45° (Fig. 2). For comparison purposes, solid injection molding specimens were fabricated using a Morgan-Press machine G-100T (Morgan Industries, Inc. Long Beach

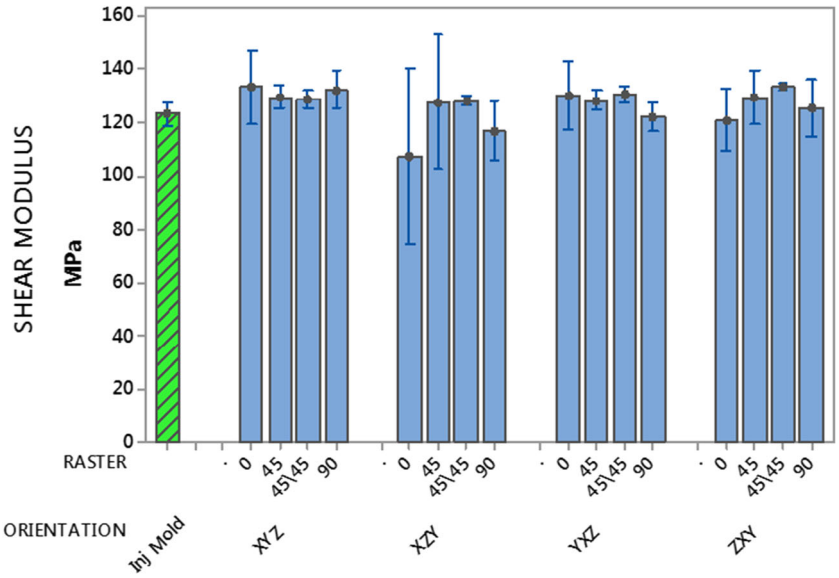

Fig. 3 Mean shear modulus with associated 95% confidence interval

Calif. USA) in a custom-machined aluminum mold. The same Stratasys ABS-M30 thermoplastic material (lot, 7677) was pelletized using a pelletizer machine (Collin, Ebersberg, Germany) and was subsequently injection molded.

To avoid fabrication errors resulting from geometry approximation of curves in FDM process, a rectangular specimen of 0.007 × 0.014 × 0.08 m was used following recommendations by ASTM D5279-13 [18]. The printed and injected specimens were conditioned following the ASTM D618 standard [19]. Air gap, layer thickness, raster width, and offset contours were constant for all printed specimens (Table 1a). Injection molding parameters are presented in Table 1b. Minitab Software was used to perform statistical analysis.

Torsional tests were performed using a MTS Landmark Bionix Servohydraulic Test System with a 250 Nm force transducer (MTS Systems Corporation, Eden Prairie, MN). A monotonic torsion test (angle of twist progressing from 0° to 270°) was performed using a data acquisition rate of 100 measurements per second. To avoid thermal effects of expansion or contraction, the speed was fixed at one degree per second at room temperature (25 ± 1 °C).

Torque, angle, and time were acquired to establish stress-strain curves. Shearing stress τ was calculated by the formula for a rectangular bar expressed in Pascal units (Pa) [20]:

$$\tau = \frac{T}{c_1 a b^2} \tag{1}$$

where T is the magnitude of the torque applied (Nm), a is the measure of the wider side of the rectangular specimen in meters (m), b is the measure of the narrower side of the cross section in meters (m), and c_1 is the coefficient associated with the ratio a/b obtained from Table 2. Shearing

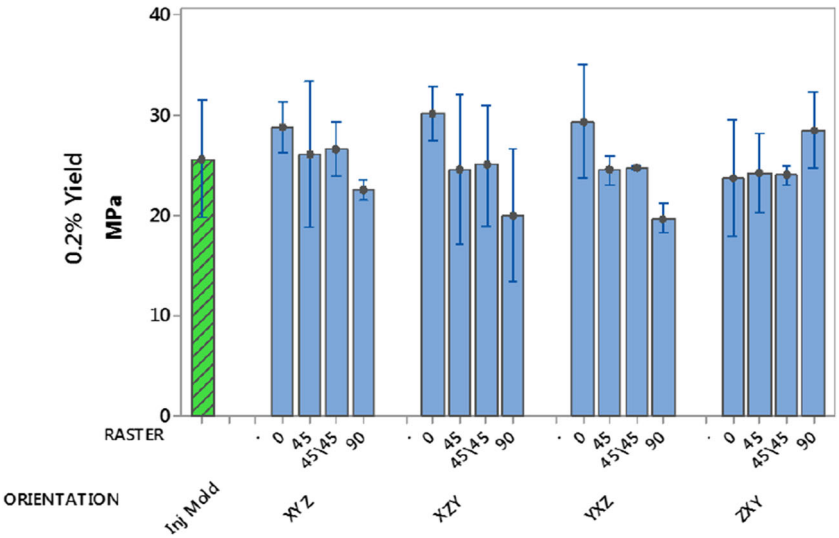

Fig. 4 0.2% yield strength in torsion for different orientation and raster angle combinations with 95% CI

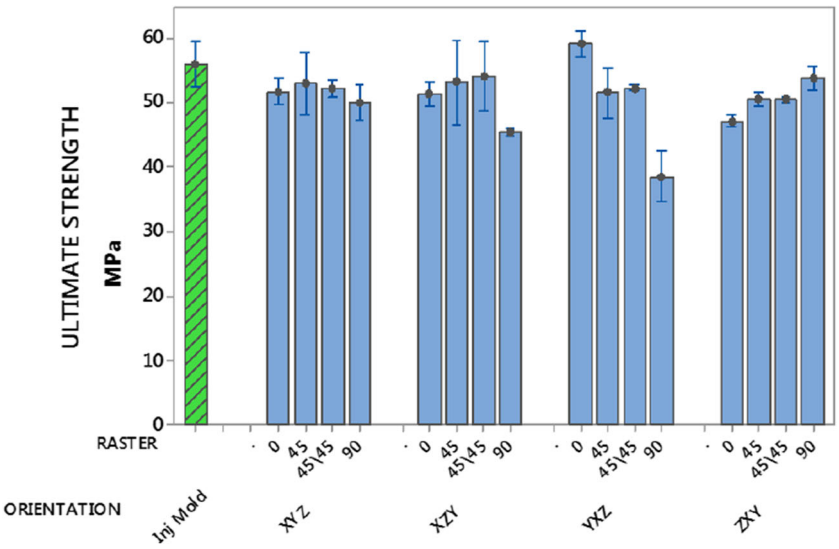

Fig. 5 Ultimate strength plot in torsion with 95% CI and intervals calculated by individual standard deviations

strain γ represents the torsion angle in radians (rad) and can be calculated by using Eq. 2 (based on [20]):

$$\gamma = \frac{C_2 b \phi}{C_1 L} \tag{2}$$

where L is the length of the specimen (m), C_1 and C_2 are the coefficients also taken from Table 2, and ϕ is the angle of twist. Then the shear modulus G can be calculated by using Eq. 3 [20]:

$$G = \frac{\tau}{\gamma} \tag{3}$$

To find the relation in Eq. 3, a linear regression is obtained from the linear behavior of the elastic region in the stress-strain curve. G is the slope of the line obtained for each combination of the factorial Design of Experiment (DOE). G can be used as a measure to compare the stiffness values of the considered combinations [21].

The 0.2% yield strength (τ_y) is considered a more precise point at which material begins plastic deformation; it was obtained from a line that was parallel to the linear curve in the elastic area with offset to the right by 0.2% of the angular displacement. This strength is the limit point where elastic deformation ends and plastic deformation begins [21].

The ultimate shear strength (US_S) was obtained from the maximum shear stress within the ductile region of stress-strain graph. In a similar manner, fracture strain (γ_f) was the strain value at which the shear stress decreased [21].

To identify the effects of orientation and raster angle in the response variables (G, US_S, τ_y, and γ_f), a general factorial analysis was performed using an ANOVA with a confidence level (CL) of 95% applied to the full design considering significance with a p value (p) below 0.05. The interaction effects of the two factors were captured in order to search for a significant response when orientation and raster angle are applied simultaneously.

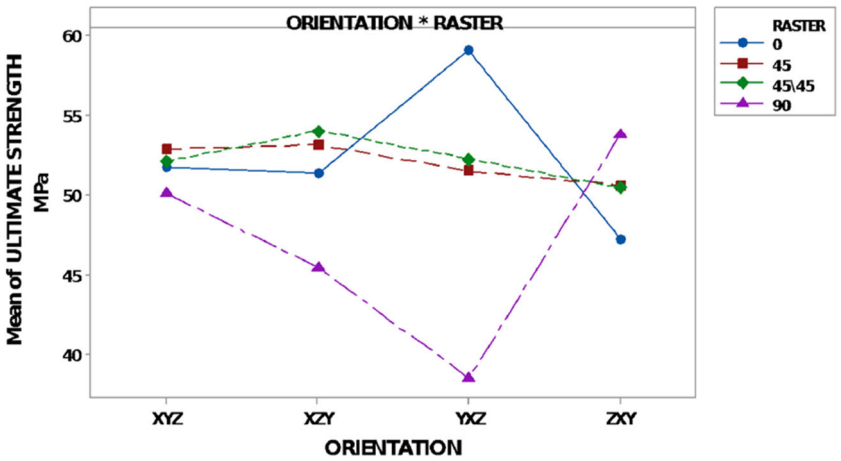

Fig. 6 Interaction of orientation and raster angle in the ultimate strength using fitted means

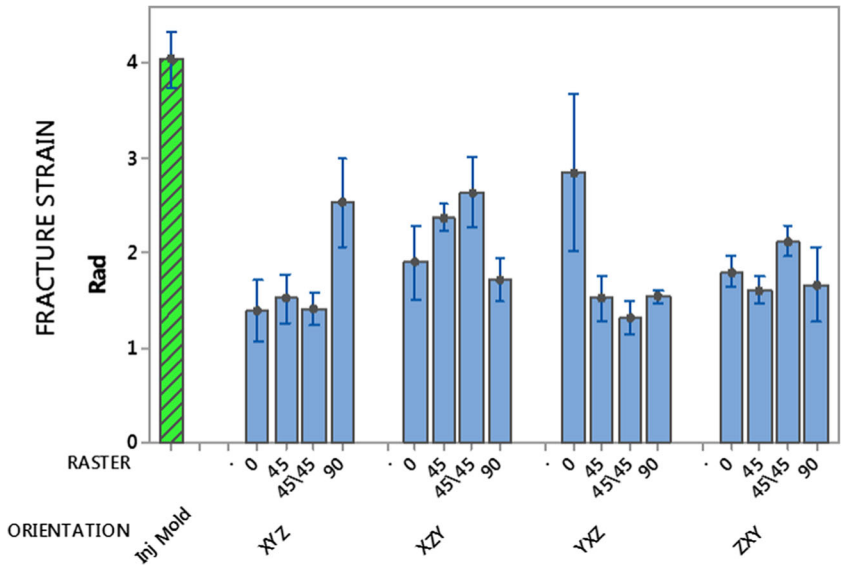

Fig. 7 Fracture strain plot in torsion with 95% CI and intervals calculated by individual standard deviations

To obtain not only the effect of the factors that produce better endurance, but also the effects of the level combinations (XYZ, YXZ, ZXY, and XZY levels with 0°, 45°, 90°, and 45/45° levels), a post hoc Bonferroni test of individual confidence intervals was used for each pairwise differences. This is a general method valid whenever several confidence intervals or tests are considered simultaneously [22]. In this direction, tests were performed in two stages: first, to test comparisons among the four levels of each factor (CL = 99.17), and second, to test each of the 16 (4^2) initial combinations by pairs plus one injection molding arrangement (${}_{17}C_2 = 136$ intervals in total) using an adjusted individual CL of 96.96% to obtain an overall CL of 95%. Finally, response optimization was used to find the set of combinations that maximized the stress and strain values in the four response variables. A desirability function in a multiple response model is explained in Section 3.5.

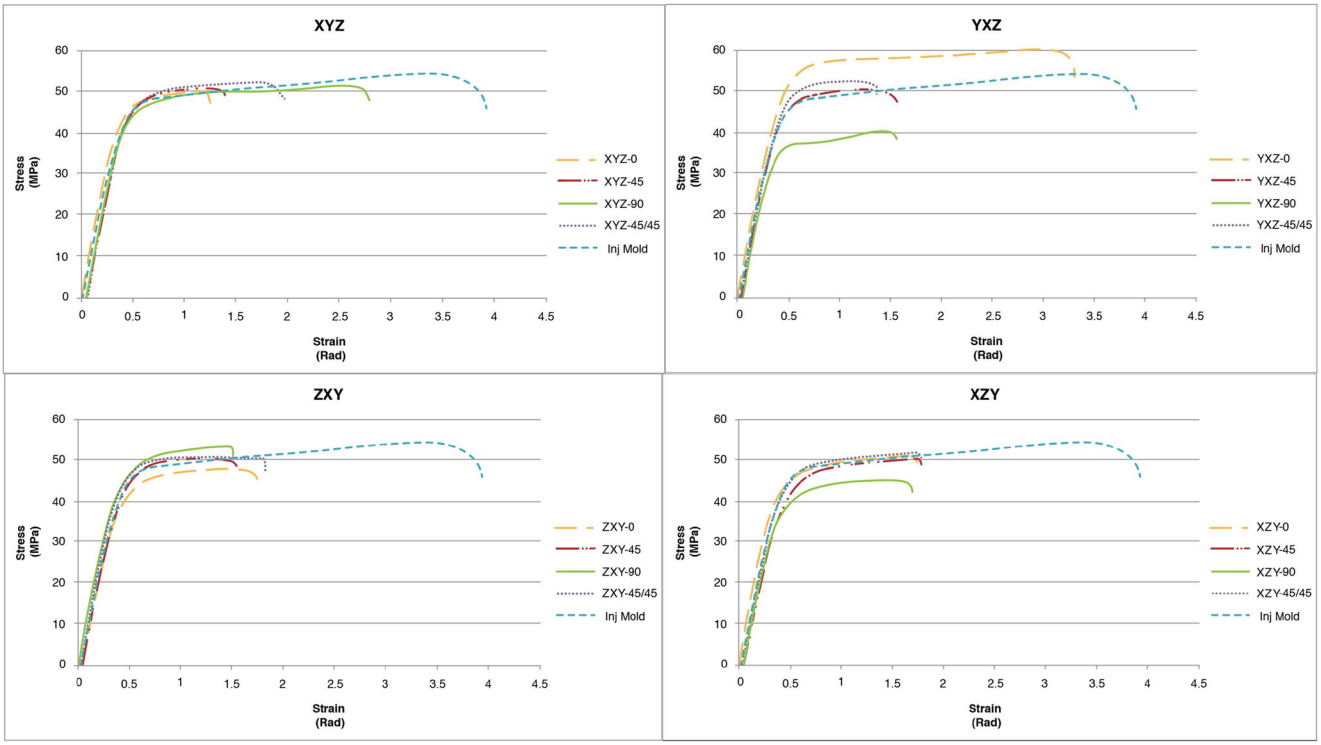

Fig. 8 Representations of the stress-strain curves grouped by the orientation of the specimen

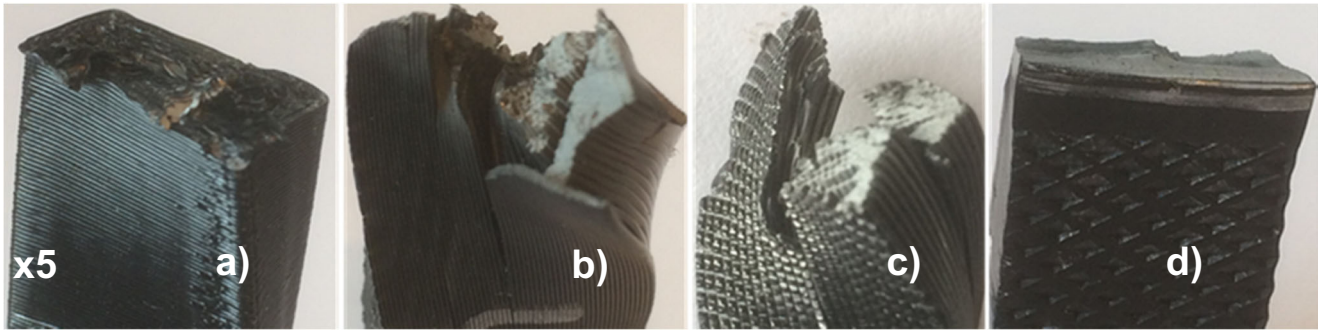

Fig. 9 Images of the physical fracture on different specimens. (**a**) ZXY-0^0 combination specimen, (**b**) XZY-0^0 combination specimen, (**c**) YXZ-90^0 combination specimen, and (**d**) Injection Molding Specimen

3 Results

Results were classified by the response variables obtained from the stress-strain analysis. Interval plots with multi-way grouping were constructed to display the mean and associated confidence intervals adjusted to reach a 95% of the CL (computed by individual standard deviations) to find differences in the orientation and raster angle combinations. Also, measurements of the injection molding specimens were added to the analysis. Expressions containing an axis orientation and an angle separated by a dash or underscore symbols (e.g., XYZ-0^0 or XYZ_0^0) mean that a specific orientation has been used with a specific raster angle (described in Figs. 1 and 2).

3.1 Shear modulus (*G*)

In order to find significant differences, a comparison between each level (e.g., group XYZ against group ZXY), and then a comparison between each individual combination of the four levels (e.g., XYZ-90^0 combination against XYZ-0^0 combination), was performed. Results for the shear modulus are presented in Fig. 3. Note that the mean shear modulus for the 16 possible combinations of orientation and raster angle were similar. Grouping information using the post hoc method showed differences within the orientation level XZY against the XYZ ($p = 0.001$) and within YXZ against XZY ($p = 0.037$), but not within the raster angle levels. The pairwise analysis for the individual comparisons only showed a significant difference in the lowest value (107.18 ± 13.252 MPa) of the XZY-0° combination (see Figs. 1 and 2), where a difference was denoted against all individual combinations except with the XZY-90° ($p = 1.000$), YXZ-90° ($p = 0.203$), and ZXY-0° ($p = 0.363$). Overall, the combinations of XYZ-0° (133.19 ± 5.555 MPa) and ZXY-45°/45° (133.39 ± 0.605 MPa) exhibited the highest means. Orientation, raster angle, and their interaction were determinant factors to modify the shear modulus variable according to the ANOVA analysis ($p = 0.000$, $p = 0.004$, and $p = 0.003$, respectively). Besides, the injection molded specimens did not present significant difference on the stress/strain compared to printed specimens.

3.2 0.2% yield strength (τ_y)

The raster angle factor and its interaction with the orientation was significant ($p = 0.004$ and $p = 0.003$, respectively) in modifying the variable of the 0.2% yield strength, as opposed to the orientation factor, where ANOVA did not show significance ($p = 0.262$). This can mean that the behavior of the two factors is different when they are used together. No differences were found in the orientation levels, but for the *raster angle* levels, a difference in 90° against 0° was relevant with a $p = 0.000$. The pairwise tests of the individual combinations, confirmed a significant difference between the combinations with high means values (XYZ-0°, XZY-0°, YXZ-0°, and ZXY-90°), against the lower means (YXZ-90°, XZY-90°, and XYZ-90°) as observed in Fig. 4. The injection molding mean (25.68 ± 2.383 MPa) only showed a difference with the YXZ-90° combination (19.747 ± 0.554 MPa) with a $p = 0.043$.

Table 3 Values for the multiple response experiment obtained from 2^4 factorial design

Variable	Target value (T_i)	Lowest acceptable value (L_i)	$\hat{Y}_i$ for YXZ-0^0
$\hat{Y}_1$ shear modulus (*G*)	138.75 MPa	92.365 Mpa	130.127 Mpa
$\hat{Y}_2$ 0.2% yield strength (τ_y)	31.989 MPa	17.038 Mpa	29.3788 Mpa
$\hat{Y}_3$ ultimate strength (US_s)	59.909 Mpa	37.191 Mpa	59.0555 Mpa
$\hat{Y}_4$ fracture strain (γ_f)	3.161 rad	1.2348 rad	2.85357 rad

Table 4 Values for the multiple response experiment obtained from 2^4 factorial design

Variable	Individual d_i	Desirability	d_i value
Shear modulus (G)	d_1=	((130.127–92.365 MPa)/(138.75–92.365 MPa))=	0.8141
0.2% yield strength (τ_y)	d_2	((29.378–17.038 MPa)/(31.989–17.0383 MPa))=	0.8254
Ultimate strength (US_s)	d_3	((59.055–37.191 MPa)/(59.909–37.191 MPa))=	0.9624
Fracture strain (γ_f)	d_4	((2.853–1.234 rad)/(3.161–1.234 rad))=	0.8402

3.3 Ultimate strength (US_S)

For ultimate strength, a difference of level 90° against 0° ($p = 0.014$) and 90° against 45° ($p = 0.024$), as well as 90° against 45°/45° was observed in the raster angle factor. For orientation, no level differences were observed. Figure 5 shows a plot for the ultimate strength where the mean of the combination YXZ-0° (59.06 ± 0.821 MPa) was the highest and had a statistically significant difference over all printed specimens except injection molding ($p = 0.574$), while YXZ-90° was the lowest ultimate strength value (38.456 ± 1.562 MPa) of the individual comparisons with a statistically significant difference from the rest of the combinations. Injection molding specimens demonstrated no significant differences in the maximum strength in relation to some printed specimens with higher values (i.e., XYZ-45°, XYZ-45°/45°, XZY-45°, XZY-45°/45°, YXZ-0°, YXZ-45°/45°, and ZXY-90°), but were significantly greater than the other printed combinations (i.e., XYZ-0°, XYZ-90°, XZY-0°, XZY-90°, YXZ-45°, YXZ-90°, ZXY-0°, ZXY-45°, and ZXY-45°/45°).

Table 5 Results of the response optimization applied to the full factorial design

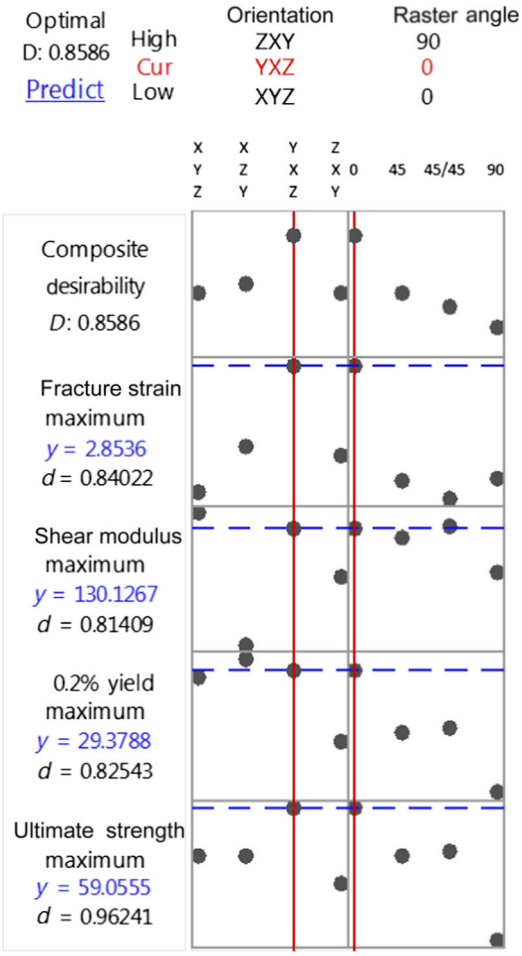

The factorial analysis demonstrates that the orientation did not affect the ultimate strength results ($p = 0.53$), whereas the raster angle and the interaction did, with a $p = 0.000$ in both cases. A graph of interaction is shown in Fig. 6, where the interaction of a 90° raster angle with XZY is notable, and YXZ orientations produce low ultimate strength values (the slope is decreasing in 90° line). In contrast, a 0° raster angle with YXZ orientation generated a higher ultimate strength.

3.4 Fracture strain (γ_f)

The fracture strains measured for injection molding (4.043 ± 0.120 rad) were remarkably different when compared to all other printed specimens in the interval plot of fracture strain (Fig. 7). The post hoc test also showed a statistical difference for injection molding. Considering only the printed specimens, no differences were detected in the fracture strain analysis. Following injection molding, YXZ-0° (2.854 ± 0.335 rad), XZY-45°/45° (2.638 ± 0.151 rad), and XYZ-90° (2.531 ± 0.190 rad) were the next best results. Orientation, raster angle, and the interaction of the two ($p = 0.000$, $p = 0.001$, and $p = 0.000$) were variables that affected the ductility behavior of the specimens with no significant differences between the levels of orientation and raster angle.

Fracture strain values were used as a measure of deformation before failure, where ductility can be observed in the strain-stress curve after the 0.2% of yield occurs [21]. Figure 8 presents the strain-strain curves of the torsion test, where we can compare representations of the mechanical behavior of the orientation, raster angle, and injection molding specimens. As we can see, compared curves seem to be similar before ultimate strength in XYZ, ZXY, and XZY orientations but not in the YXZ orientation. Difference in the plasticity property of the injection molded specimens is remarkable in the four graphs (see strain axis), and only the orientation

YXZ-0° was superior in the stress (MPa) results against injection molding specimens.

According to the results obtained for the four variables (G, US_S, τ_y, and γ_f), no perpendicular or parallel angle association of rasters was detected against the direction of the torsion force to obtain better strength; an orthogonal direction of the raster-generated high values (e.g., XYZ-0° on G, XZY-0° on US_S) but also a parallel raster against the force (e.g., YXZ-0° on US_S, τ_y, and γ_f). A crossed pattern in rasters (45°/45°) also obtained higher results when compared against other combinations (e.g., ZXY-45°/45° on G and US_S). An exposed fracture was observed (Fig. 9) and a plane cutting line was presented on specimens with printed layers in the same plane of the force (Fig. 9a), while specimens with no apparent specific cutting shape were presented when rasters were in different directions against the torsion force (Fig. 9b, c). Again, no angle against force was identified as better in relation with stress-strain results.

3.5 Variables optimization

Using the data from the previous 2^4 factorial design, an optimization model was applied to find the combinations of orientation-raster angle levels to maximize stress and strain values. Following functions proposed by Derringer and Suich [23], a multiple response model was utilized based on the individual desirability function to maximize a response (Eq. 4), and the composite desirability, with the same importance for each response (Eq. 5).

$$d_i = \begin{cases} 0 & \hat{Y}_i < L_i \\ \left(\frac{\hat{Y}_i - L_i}{T_i - L_i}\right) & L_i \le T_i \\ 0 & \hat{Y}_i < T_i \end{cases} \quad (4)$$

where:

- $\hat{Y}_i$ Predicted value of i^{th} response
- T_i Target value of i^{th} response
- L_i Lowest acceptable value for i^{th} response
- d_i Desirability for i^{th} response
- r_i Weight of desirability function of i^{th} response

Thus, the formula for composite desirability (D) with the same importance for each response is:

$$D = (d_1 \times d_i \times \ldots \times d_i)^{1/n} \quad (5)$$

As the multiple response experiment is a maximizing approach, the target value (T_i) for each of the responses in Eq. 4 was obtained from the maximum value of the runs in the factorial design (Figs. 3, 4, 5, and 7 show the mean and standard deviation on each run). Similarly, the lowest acceptable values (L_i) were detected from the lowest values using the statistical software. Table 3 presents the obtained values.

Predicted values ($\hat{Y}_i$) in Table 3 were calculated from the regression equations in the ANOVA analysis performed in Section 3. The equations computed by the software utilized to find differences between the orientation and raster angle factors are in Eqs. 6, 7, 8, and 9.

$$\begin{aligned} \text{Shear modulus} = {} & 126.348 + 4.45\ \text{XYZ} - 6.51\ \text{XZY} \\ & + 1.25\ \text{YXZ} + 0.81\ \text{ZXY} - 3.55\ 0^0 \\ & + 2.23\ 45^0 + 3.77\ 45^0\backslash 45^0 - 2.45\ 90^0 \\ & + 5.94\ \text{XYZ\_}0^0 - 3.62\ \text{XYZ\_}45^0 \\ & - 5.97\ \text{XYZ\_}45^0\backslash 45^0 \\ & + 3.65\ \text{XYZ\_}90^0 - 9.11\ \text{XZY\_}0^0 \\ & + 5.40\ \text{XZY\_}45^0 \\ & + 4.38\ \text{XZY\_}45^0\backslash 45^0 - 0.68\ \text{XZY\_}90^0 \\ & + 6.08\ \text{YXZ\_}0^0 - 1.67\ \text{YXZ\_}45^0 \\ & - 0.87\ \text{YXZ\_}45^0\backslash 45^0 - 3.54\ \text{YXZ\_}90^0 \\ & - 2.91\ \text{ZXY\_}0^0 - 0.11\ \text{ZXY\_}45^0 \\ & + 2.46\ \text{ZXY\_}45^0\backslash 45^0 \\ & + 0.57\ \text{ZXY\_}90^0 \end{aligned} \quad (6)$$

$$\begin{aligned} 0.2\%\text{yield} = {} & 25.199 \\ & + 0.846\ \text{XYZ} - 0.214\ \text{XZY} - 0.577\ \text{YXZ} \\ & - 0.055\ \text{ZXY} \\ & + 2.830\ 0^0 - 0.316\ 45^0 - 0.059\ 45^0\backslash 45^0 \\ & - 2.455\ 90^0 - 0.033\ \text{XYZ\_}0^0 \\ & + 0.430\ \text{XYZ\_}45^0 \\ & + 0.616\ \text{XYZ\_}45^0\backslash 45^0 - 1.014\ \text{XYZ\_}90^0 \\ & + 2.353\ \text{XZY\_}0^0 - 0.036\ \text{XZY\_}45^0 \\ & + 0.126\ \text{XZY\_}45^0\backslash 45^0 - 2.443\ \text{XZY\_}90^0 \\ & + 1.928\ \text{YXZ\_}0^0 + 0.215\ \text{YXZ\_}45^0 \\ & + 0.276\ \text{YXZ\_}45^0\backslash 45^0 - 2.419\ \text{YXZ\_}90^0 \\ & - 4.248\ \text{ZXY\_}0^0 - 0.610\ \text{ZXY\_}45^0 \\ & - 1.018\ \text{ZXY\_}45^0\backslash 45^0 + 5.876\ \text{ZXY\_}90^0 \end{aligned} \quad (7)$$

$$\begin{aligned}\text{Ultimate strength} = {} & 50.858 + 0.811\ \text{XYZ} \\ & + 0.123\ \text{XZY} - 0.548\ \text{YXZ} - 0.386\ \text{ZXY} \\ & + 1.464\ 0^0 + 1.147\ 45^0 \\ & + 1.320\ 45^0\backslash 45^0 - 3.932\ 90^0 \\ & - 1.442\ \text{XYZ\_}0^0 + 0.026\ \text{XYZ\_}45^0 \\ & - 0.900\ \text{XYZ\_}45^0\backslash 45^0 \\ & + 2.316\ \text{XYZ\_}90^0 - 1.053\ \text{XZY\_}0^0 \\ & + 0.992\ \text{XZY\_}45^0 \\ & + 1.694\ \text{XZY\_}45^0\backslash 45^0 \\ & - 1.633\ \text{XZY\_}90^0 + 7.280\ \text{YXZ\_}0^0 \\ & + 0.042\ \text{YXZ\_}45^0 \\ & + 0.601\ \text{YXZ\_}45^0\backslash 45^0 \\ & - 7.923\ \text{YXZ\_}90^0 - 4.786\ \text{ZXY\_}0^0 \\ & - 1.060\ \text{ZXY\_}45^0 - 1.395\ \text{ZXY\_}45^0\backslash 45^0 \\ & + 7.240\ \text{ZXY\_}90^0 \end{aligned} \quad (8)$$

$$\begin{aligned}\text{Fracture strain} = {} & 1.8701 - 0.1558\ \text{XYZ} \\ & + 0.2877\ \text{XZY} - 0.0634\ \text{YXZ} \\ & - 0.0685\ \text{ZXY} \\ & + 0.1183\ 0^0 - 0.1159\ 45^0 \\ & + 0.0038\ 45^0\backslash 45^0 - 0.0062\ 90^0 \\ & - 0.4398\ \text{XYZ\_}0^0 - 0.0794\ \text{XYZ\_}45^0 \\ & - 0.3039\ \text{XYZ\_}45^0\backslash 45^0 \\ & + 0.8232\ \text{XYZ\_}90^0 - 0.3723\ \text{XZY\_}0^0 \\ & + 0.3302\ \text{XZY\_}45^0 \\ & + 0.4769\ \text{XZY\_}45^0\backslash 45^0 \\ & - 0.4347\ \text{XZY\_}90^0 \\ & + 0.9285\ \text{YXZ\_}0^0 - 0.1723\ \text{YXZ\_}45^0 \\ & - 0.4960\ \text{YXZ\_}45^0\backslash 45^0 \\ & - 0.2602\ \text{YXZ\_}90^0 - 0.1164\ \text{ZXY\_}0^0 \\ & - 0.0784\ \text{ZXY\_}45^0 \\ & + 0.3231\ \text{ZXY\_}45^0\backslash 45^0 \\ & - 0.1282\ \text{ZXY\_}90^0 \end{aligned} \quad (9)$$

To find the predicted value ($\hat{Y}_i$) on each equation, zero (0) or one (1) is assigned instead of the variable according to the presence/no presence of the orientation and raster angle combination (e.g., in XZY_ 90^0, set the variable to one for each containing XZY, 90^0 or both. The other variables would be set to zero). Then a series of iterations were performed to find the combination that obtained the higher value on each regression equation. The best values found in Table 3 represent the results of the YXZ-0^0 combination.

Using the values of Table 3 and the formula of Eq. 4, the individual desirability was computed, considering the same weight for all responses (see Table 4).

Then, the composite desirability (D) presented in Eq. 5 was used, with the individual values shown in Table 4:

$$D = (0.8141 \times 0.8254 \times 0.9624 \times 0.8402)^{1/4} = 0.8586$$

Table 5 presents a summary of the software calculations showing the optimal values for combinations; vertical lines cross the points where values can be maximized for each of the mechanical properties of the ABS in torsion. Each variable features the composite desirability value (d) and the individual response (Y) calculated. Also, an optimal solution in the YXZ-0^0 combination was obtained.

4 Conclusions

According to the torsion results of this research, thermoplastic ABS-M30 printing using the FDM process shows no significant difference when compared to injection molding while considering results in: shear modulus, ultimate shear strength, and 0.2% yield strength. However, a notable difference was detected when comparing fracture strain. This difference may indicate that the FDM process can print components with similar elastic properties in torsion, but with less ductility than injection molding components.

An interaction effect of factors was present in all the independent response variables (G, US_S, τ_y, and γ_f) since the orientation and the raster angle can produce different results when applied at the same time rather than when applied separately. This interaction could cause a stronger anisotropic behavior resulting in difficulties to establish a confident arrangement for prognostic stress-strain results in printed objects that are under torsion force. In spite of this, the experiment presented remarkable observations: The orientation did not significantly modify the response variable either in the ultimate shear strength or in the 0.2% yield strength. Comparing only printed specimens, the XZY-0^o combination resulted in significantly reduced shear modulus; the XZY-90^o and YXZ-90^o had reduced values when considering the 0.2% yield strength, as well as YXZ-90^o in the ultimate strength. Using an optimization factorial model, the orientation in YXZ with rasters at 0^o resulted in improved responses in all measured torsion variables (G, US_S, τ_y, and γ_f). This result is

consistent with comparisons made through statistical and graphical analysis. Due to the difference in the material composition, the reproduction of this experiment using other kinds of ABS material can produce different levels of endurance, but the process behavior should be similar.

Acknowledgements This work was supported by the University of Texas at El Paso (UTEP) within the W.M. Keck Center for 3D Innovation in collaboration with the Universidad Autónoma de Ciudad Juarez (Autonomous University of Ciudad Juárez).

References

1. Gartner (2016) Gartner Says Worldwide Shipments of 3D Printers to Grow 108 Percent in 2016. http://www.gartner.com/newsroom/id/3476317. Accessed 17 Nov 2017
2. ASTM F2792-12a (2012) Standard terminology for additive manufacturing technologies. ASTM International, West Conshohocken
3. Torres J, Cotelo J, Karl J, Gordon AP (2015) Mechanical property optimization of FDM PLA in shear with multiple objectives. JOM 67(5):1183–1193. https://doi.org/10.1007/s11837-015-1367-y
4. Croccolo D, De Agostinis M, Olmi G (2013) Experimental characterization and analytical modelling of the mechanical behavior of fused deposition processed parts made of ABS-M30. Comput Mater Sci 79:506–518. https://doi.org/10.1016/j.commatsci.2013.06.041
5. Bellini A, Güçeri S (2003) Mechanical characterization of parts fabricated using fused deposition modeling. Rapid Prototyp J 9(4):252–264. https://doi.org/10.1108/13552540310489631
6. Ziemian C, Sharma M, Ziemian S (2012) Anisotropic mechanical properties of ABS parts fabricated by fused deposition modelling. Mech Eng. https://doi.org/10.5772/34233
7. Hossain MS, Espalin D, Ramos J, Perez M, Wicker R (2014) Improved mechanical properties of fused deposition modeling-manufactured parts through build parameter modifications. J Manuf Sci Eng 136(6):061002. https://doi.org/10.1115/1.4028538
8. Sood AK, Ohdar RK, Mahapatra SS (2010) Parametric appraisal of mechanical property of fused deposition modelling processed parts. Mater Des 31(1):287–295. https://doi.org/10.1016/j.matdes.2009.06.016
9. Lee CS, Kim SG, Kim HJ, Ahn SH (2007) Measurement of anisotropic compressive strength of rapid prototyping parts. J Mater Process Technol 187-188:627–630. https://doi.org/10.1016/j.jmatprotec.2006.11.095
10. Ahn S, Montero M, Odell D, Roundy S, Wright PK (2002) Anisotropic material properties of fused deposition modeling ABS. Rapid Prototyp J 8(4):248–257. https://doi.org/10.1108/13552540210441166
11. Wu W, Geng P, Li G, Zhao D, Zhang H, Zhao J (2015) Influence of layer thickness and raster angle on the mechanical properties of 3D-printed PEEK and a comparative mechanical study between PEEK and ABS. Materials 8(9):5834–5846. https://doi.org/10.3390/ma8095271
12. Lee BH, Abdullah J, Khan ZA (2005) Optimization of rapid prototyping parameters for production of flexible ABS object. J Mater Process Technol 169(1):54–61. https://doi.org/10.1016/j.jmatprotec.2005.02.259
13. Roberson DA, Torrado Perez AR, Shemelya CM, Rivera A, MacDonald E, Wicker RB (2015) Comparison of stress concentrator fabrication for 3D printed polymeric izod impact test specimens. Additive Manufacturing 7:1–11. https://doi.org/10.1016/j.addma.2015.05.002
14. Es-Said OS, Foyos J, Noorani R, Mendelson M, Marloth R, Pregger BA (2000) Effect of layer orientation on mechanical properties of rapid prototyped samples. Mater Manuf Process 15(1):107–122. https://doi.org/10.1080/10426910008912976
15. Anitha R, Arunachalam S, Radhakrishnan P (2001) Critical parameters influencing the quality of prototypes in fused deposition modelling. J Mater Process Technol 118(1-3):385–388. https://doi.org/10.1016/s0924-0136(01)00980-3
16. ASTM F2921-11 (2011) Standard terminology for additive manufacturing coordinate systems and test methodologies. ASTM International, West Conshohocken
17. Riley W, Sturges L, Morris D (2006) Mechanics of materials. John Wiley & Sons, Hoboken
18. ASTM D5279-13 (2013) Standard practice for conditioning plastics for testing. ASTM International, West Conshohocken
19. ASTM D618-13 (2013) Standard test method for plastics: dynamic mechanical properties: in torsion. ASTM International, West Conshohocken
20. Beer FP, Johnston ER, DeWolf JT, Mazurek DF (2012) Mechanics of materials. McGraw-Hill Engineering Series, New York
21. Fitzgerald RW (1982) Mechanics of materials. Addison-Wesley, Reading
22. Navidi W (2006) Statistics for engineers and scientists. McGraw-Hill, New York
23. Derringer G, Suich R (1980) Simultaneous optimization of several response variables. J Qual Technol 12:214–219